




# Simultaneous high-resolution whole-brain MR spectroscopy and [<sup>18</sup>F] FDG PET for temporal lobe epilepsy

Hui Huang<sup>1</sup> · Miao Zhang<sup>2</sup> · Yibo Zhao<sup>3,4</sup> · Yudu Li<sup>3,5</sup> · Wen Jin<sup>3,4</sup> · Rong Guo<sup>3,6</sup> · Wei Liu<sup>7</sup> · Bingyang Cai<sup>1</sup> · Jiwei Li<sup>1</sup> · Siyu Yuan<sup>1</sup> · Xinyun Huang<sup>2</sup> · Xiaozhu Lin<sup>2</sup> · Zhi-Pei Liang<sup>3,4</sup> · Biao Li<sup>2</sup> · Jie Luo<sup>1</sup> 

Received: 23 July 2023 / Accepted: 28 September 2023 / Published online: 12 October 2023  
© The Author(s), under exclusive licence to Springer-Verlag GmbH Germany, part of Springer Nature 2023

## Abstract

**Purpose** Precise lateralizing the epileptogenic zone in patients with drug-resistant mesial temporal lobe epilepsy (mTLE) remains challenging, particularly when routine MRI scans are inconclusive (MRI-negative). This study aimed to investigate the synergy of fast, high-resolution, whole-brain MRSI in conjunction with simultaneous [<sup>18</sup>F]FDG PET for the lateralization of mTLE.

**Methods** Forty-eight drug-resistant mTLE patients (M/F 31/17, age 12–58) underwent MRSI and [<sup>18</sup>F]FDG PET on a hybrid PET/MR scanner. Lateralization of mTLE was evaluated by visual inspection and statistical classifiers of metabolic mappings against routine MRI. Additionally, this study explored how disease status influences the associations between altered N-acetyl aspartate (NAA) and FDG uptake using hierarchical moderated multiple regression.

**Results** The high-resolution whole-brain MRSI data offers metabolite maps at comparable resolution to [<sup>18</sup>F]FDG PET. Visual examinations of combined MRSI and [<sup>18</sup>F]FDG PET showed an mTLE lateralization accuracy rate of 91.7% in a 48-patient cohort, surpassing routine MRI (52.1%). Notably, out of 23 MRI-negative mTLE, combined MRSI and [<sup>18</sup>F]FDG PET helped detect 19 cases. Logistical regression models combining hippocampal NAA level and FDG uptake improved lateralization performance (AUC=0.856), while further incorporating extrahippocampal regions such as amygdala, thalamus, and superior temporal gyrus increased the AUC to 0.939. Concurrent MRSI/PET revealed a moderating influence of disease duration and hippocampal atrophy on the association between hippocampal NAA and glucose uptake, providing significant new insights into the disease's trajectory.

**Conclusion** This paper reports the first metabolic imaging study using simultaneous high-resolution MRSI and [<sup>18</sup>F]FDG PET, which help visualize MRI-unidentifiable lesions and may thus advance diagnostic tools and management strategies for drug-resistant mTLE.

**Keywords** PET/MRSI · N-Acetyl aspartate · Glucose · Temporal lobe epilepsy · Lateralization

---

Hui Huang and Miao Zhang contributed equally to this work.

✉ Biao Li  
lb10363@rjh.com.cn

✉ Jie Luo  
jieluo@sjtu.edu.cn

<sup>1</sup> School of Biomedical Engineering, Shanghai Jiao Tong University, Shanghai 200240, China

<sup>2</sup> Department of Nuclear Medicine, Ruijin Hospital, Shanghai Jiao Tong University School of Medicine, Shanghai 200025, China

<sup>3</sup> Beckman Institute for Advanced Sciences and Technology, University of Illinois at Urbana Champaign, Urbana, IL 61801, USA

<sup>4</sup> Department of Electrical and Computer Engineering, University of Illinois at Urbana Champaign, Urbana, IL 61801, USA

<sup>5</sup> National Center for Supercomputing Applications, University of Illinois at Urbana Champaign, Urbana, IL 61801, USA

<sup>6</sup> Siemens Medical Solutions USA, Inc, Urbana, IL 61801, USA

<sup>7</sup> Department of Neurosurgery, Ruijin Hospital, Shanghai Jiao Tong University School of Medicine, Shanghai 200025, China

## Introduction

Epilepsy is one of the most common neurological disorders that occurs in 1% population worldwide [1]. The majority of drug-resistant epilepsy patients in need of surgical intervention are mesial temporal lobe epilepsy (mTLE) [2]. Precise lateralization of the epileptogenic zone (EZ), which is commonly associated with hippocampal sclerosis (HS) characterized by neuronal damage and reactive gliosis [3, 4], is crucial in the pre-surgical evaluation of mTLE. However, routine MRI examinations fail to identify lesions in approximately 33% of mTLE patients (so-called MRI-negative cases) [5]. These cases require more comprehensive presurgical examinations in tertiary centers, and face a higher risk of post-surgical seizure recurrence [6]. There is a pressing need for neuroimaging techniques more sensitive to subtle lesions in MRI-negative patients to better guide intracranial electroencephalography (icEEG) during the presurgical evaluation and potentially improve surgical outcomes [7, 8].

Molecular changes have been shown to present early, sensitive to emerging lesions prior to the formation of chronic epileptics [9, 10], and structural abnormalities [11–13]. 2- $^{18}\text{F}$ fluoro-2-deoxy-D-glucose ( $^{18}\text{F}$ FDG) PET imaging has been widely adopted in presurgical evaluation of focal epilepsy, and has been shown to help improve surgical outcome of MRI-negative patients [14, 15]. On the other hand, the reported EZ detection rate by  $^{18}\text{F}$ FDG PET varies from 60–73% [16], possibly as a result of subtle or extended interictal hypometabolism.

Magnetic resonance spectroscopy and spectroscopic imaging (MRS/I) capture multiple metabolites in a single scan, such as N-acetyl aspartate (NAA), creatine (Cr), choline (Cho), myoinositol (mIn), glutamate (Glu), glutamine (Gln), gamma-aminobutyric acid (GABA), etc. [17–20]. Previous studies had revealed consistent NAA reductions in epileptic lesions due to neuronal dysfunction [21–23]. However, conventional MRS approaches, known for their technical limitations such as long data acquisition time, low signal-to-noise ratio (SNR), low spatial resolution (over 20 mm for single voxel and over 10 mm for 2D MRSI), had mostly allowed investigations of metabolite profiles of combined mesial temporal structures per single-voxel [12, 20, 24], with sparse exploration of extratemporal metabolic alterations [25–29]. Accumulating evidence is showing abnormalities in broad epileptogenic networks of mTLE [30, 31], which emphasize the necessity of employing whole-brain high-resolution techniques in mTLE imaging.

The emergence of hybrid PET/MR scanners presents remarkable opportunity for the simultaneous assessment of glucose uptake and intrinsic neuronal metabolites such as NAA. Previously, Lee et al. reported in lithium-pilocarpine

animal model that FDG uptake, NAA, and Cho, reflecting glucose metabolism and neurochemical levels, revealed divergent course of evolution along the acute, sub-acute, and chronic stages of epileptogenesis [9]. The possibility of simultaneous  $^{18}\text{F}$ FDG PET and MRS/I imaging of human brain largely eliminate confounding physiological fluctuations [32–34], which could offer a comprehensive view of neurometabolic profile, facilitating the exploration of imaging markers in epileptic lesion detection and disease progression.

Enabled by a new MRSI technique known as Spectroscopic Imaging by exploiting spatio-spectral Correlation (referred to hereafter as SPICE) [35–39], it is feasible to obtain rapid, high-resolution, 3D metabolic imaging of the whole brain. Some related works have shown the feasibility and potential of SPICE in extracting cerebral metabolic information in stroke [40, 41] and tumor [42]. In this study, using a hybrid PET/MR scanner, we obtained 3D MRSI at the nominal resolution of  $2.0 \times 3.1 \times 2.7$  (or 3.8)  $\text{mm}^3$  within 9–12 min, simultaneously with  $^{18}\text{F}$ FDG PET from drug-resistant mTLE patients. We investigated the combined utility of high-resolution NAA map and  $^{18}\text{F}$ FDG PET at comparable spatial resolution for lateralization of mTLE compared with routine MRI, utilizing both visual inspection and statistical classifiers, incorporating extrahippocampal regions as part of epileptogenic network. Additionally, we explored the influence of disease status on the associations between altered NAA levels and FDG uptake, unveiling novel insights into epilepsy progression.

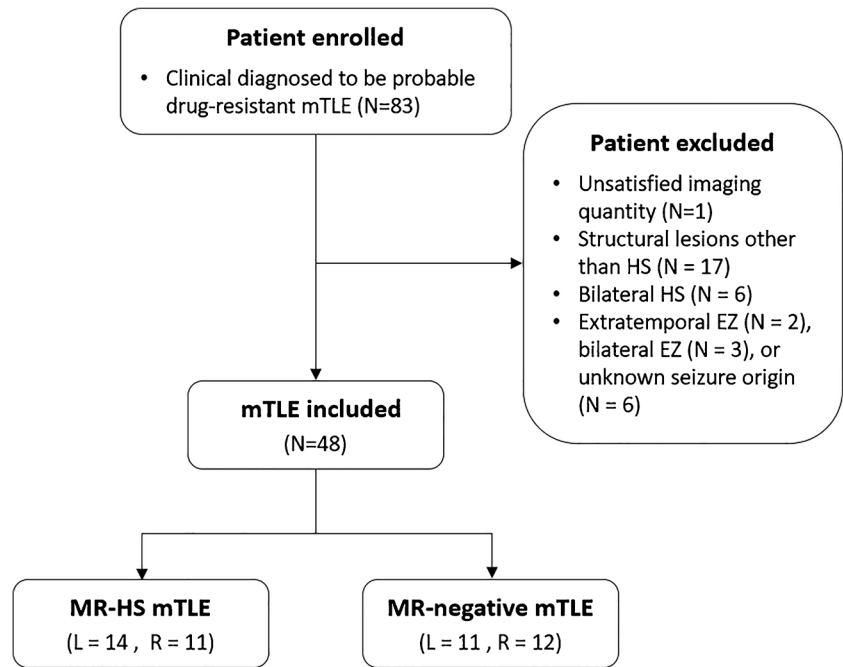
## Materials and methods

### Participants

This study has been approved by the Internal Review Board of Ruijin Hospital, Shanghai Jiao Tong University School of Medicine (Approved No. 2016-128). All patients' clinical semiology, seizure onset age, duration of the disease, and seizure frequency were collected. The laterality of the seizure focus was determined through the comprehensive evaluation, including scalp video-EEG (at least 96 h), MRI,  $^{18}\text{F}$ FDG PET, and neuropsychological testing, and where available stereo-electroencephalography (SEEG) examinations and post-operative histology of resected tissues in operated patients.

The patient inclusion flowchart is shown in Fig. 1. The inclusion criteria of patients are as follows: (1) clinical history, neurological examination, seizure semiologies, scalp video-EEG findings, and neuropsychological deficit pattern that are consistent with the characteristics of unilateral mTLE; (2) MRI either normal or disclosed patterns suggestive of HS. Exclusion criteria included: (1) generalized

**Fig. 1** Workflow of patient inclusion. HS, hippocampal sclerosis; L, left; mTLE, mesial temporal lobe epilepsy; R, right; SEEG, stereoelectroencephalography; EZ, epileptogenic zone



epilepsy syndromes; (2) posttraumatic epilepsy, brain tumor or other neurological system lesions; (3) extratemporal EZ, bilateral EZ, or unknown seizure origin; (4) patients with missing scans or poor-quality images. Finally, 48 patients were included. Among them, 34 patients had conclusive SEEG, subsequent surgery, and pathological confirmation, while the remaining 14 patients chose not to go through surgery or SEEG evaluation. The age- and gender-matched healthy control (HC) group consisted of 36 subjects. None of the healthy participants had any history of neurologic or psychiatric illness or has taken chronic medications. Written informed consents were obtained from all participants.

## Data acquisition

MRI, MRSI, and PET scans were synchronously performed with an integrated 3.0 T hybrid PET/MR system (Biograph mMR; Siemens Healthcare, Erlangen, Germany). The acquisition workflow of PET/MR scan is summarized in Supplementary Fig. 1. Patients were monitored and confirmed to have no seizures within 24 h before the scans. All subjects were required to fast for 4–6 h before the PET/MR scan, and maintained awake with their eyes closed, throughout the scan.

## MRI

MRI sequences included 3D T1-weighted anatomical images using MPRAGE (resolution  $0.5 \times 0.5 \times 1.0 \text{ mm}^3$ , TR/TE/ TI 1900/2.44/900 ms, FOV  $250 \times 250 \text{ mm}^2$ , 192 slices),

T2-weighted FLAIR (resolution  $0.4 \times 0.4 \times 3.0 \text{ mm}^3$ , TR/ TE/TI 8460/92/2433 ms, FOV  $220 \times 220 \text{ mm}^2$ , 45 slices).

## MRSI

High-resolution 3D metabolic imaging was performed using the SPICE MRSI sequence that covered an FOV of  $240 \times 240 \times 96 \text{ mm}^3$  with  $2.0 \times 3.1 \times 2.7 \text{ mm}^3$  or  $240 \times 240 \times 160 \text{ mm}^3$  with  $2.0 \times 3.1 \times 3.8 \text{ mm}^3$  nominal spatial resolution in 9 min 36 s or 12 min 35 s [38, 39], using scanner built-in automatic frequency and transmitter adjustments, as well as static field shimming right before acquisition. Briefly, in data acquisition, excitation pulses were applied without any water or lipid suppression; free induction decays were captured using fast echo-planar readouts; short TR (160 ms) was chosen for rapid imaging speed, and ultrashort TE (1.6 ms) was used to maximize SNR; interleaved navigators were acquired to track magnetic field drift and subject motions.

In data processing, subject head motion and magnetic field drifts that occurred during the MRSI scan were detected and corrected using navigator signals. High-resolution field maps were determined from the water signals and used for magnetic field inhomogeneity induced frequency shifts correction. The spatiospectral function was reconstructed from the acquired data using a union-of-subspaces model, incorporating pre-learned spectral basis functions [37–39, 43, 44]. Spectral quantification was done using an improved LCmodel-based algorithm that incorporated both spatial and

spectral priors [37]. The estimated metabolite concentrations were normalized using the water reference to compensate for the B1 inhomogeneity of the head coil used in the experiment. A more detailed description of SPICE is provided in the Supplementary Table 1 in line with the MRSinMRS Reporting Checklist [45].

### [<sup>18</sup>F]FDG PET

All patients and controls were administered [<sup>18</sup>F]FDG intravenously using a mean dose of  $184.8 \pm 29.0$  MBq (range 133.2–247.9 MBq), with the scan being initiated 30–50 min after the injection. Static PET data were acquired in a sinogram mode for 15 min, matrix size  $344 \times 344$ , and post-filtered with an isotropic Gaussian kernel of 2 mm full-width half-maximum (FWHM). The PET attenuation correction was performed using a unique 5-compartment model including bones [46]. The FDG standard uptake value ratios (SUVs) from PET images were obtained by intensity normalization via global mean scaling to correct individual variations [47].

## Data pre-processing

### ROI definition

The brain regions were automatically segmented from the T1-weighted image with the FreeSurfer v7.0 package (<https://surfer.nmr.mgh.harvard.edu>). Using the Desikan-Killiany atlas, we extracted 30 regions of interest (ROIs) from the temporal-limbic networks and seizure-relevant areas for further analysis [25, 30, 48], including 12 subcortical ROIs (left and right hippocampus, amygdala, thalamus, putamen, caudate, and pallidum) and 18 cortical ROIs (left and right inferior temporal, middle temporal, superior temporal gyrus, entorhinal, parahippocampal, transversetemporal cortices, fusiform, temporal pole and insula).

### Registration

The T1-weighted images, the SUVR maps, and the corresponding ROI masks were coregistered to the MRSI images space. Specifically, T1-weighted images were registered to MRSI images space in reference to high-resolution SPICE water image. The SUVR maps were also registered to MRSI images using the T1-weighted image as the intermediate registration reference. These registrations were employed with affine transformation through the ANTs toolkit (<http://stnava.github.io/ANTs/>).

### Voxel-based z-score metabolic map generation

Voxel-wise metabolic concentration maps were derived from spectral quantification results. We further generated the

NAA/Cr ratio map, using Cr as reference. Patient-specific metabolic ratio maps and z-score maps were processed (Supplementary Fig. 2). Original metabolic maps were masked to alleviate cerebrospinal fluid (CSF) contaminations and then were spatially normalized into the Montreal Neurological Institute (MNI) space with the registered T1-weighted image in MRSI space as the intermediate registration reference. All normalized images were smoothed with Gaussian kernels (8 mm FWHM). The z-score maps were generated by performing bootstrapping, a process of sampling with replacement, which was repeated 1000 times, to compare the patients with healthy controls. Afterward, we extracted the z-score maps of cerebral cortices and subcortical nuclei.

## Visual assessment for lateralization

All images were visually analyzed by three experienced radiologists with certificates in both nuclear medicine and radiology. Readers were blinded for the clinical diagnosis of lateralization.

### Routine MRI visual assessment

The MR images (T1-weighted, FLAIR, and T2-weighted images, with 2D axial and coronal views) were visually analyzed. MRI criteria indicative of HS included (1) atrophy of the hippocampus and/or morphology abnormalities of mesial temporal structures on T1-weighted, FLAIR, and T2-weighted images and (2) hyperintensity of the hippocampus or amygdala on FLAIR or T2-weighted images. Other minor findings associated with HS, including dilatation of the temporal horns, loss of hippocampal head interdigitations, blurry gray and white matter demarcation in the temporal pole, and atrophy of the fornix, were also taken into consideration. A patient was classified as MRI-HS if the MR images were presented with evidence of HS; and as MRI-negative if the MR images looked normal.

### MRSI visual assessment

MRSI derived maps were shown in coronal and transverse views. We mainly compared the asymmetry of bilateral hippocampus, amygdala, and temporal lobe. The hippocampus or temporal lobe that showed a lower NAA level than the opposite side was defined as positive. We combined NAA/Cr and NAA/Cr z-score results to determine patient's laterality.

### [<sup>18</sup>F]FDG PET visual assessment

PET images were divided into several zones (left and right frontal, temporal, parietal, and occipital lobe) with rainbow grading, and each zone with at least one well-defined PET hypometabolic focus was classified as positive. In PET

z-score analysis, z-score decreasing clusters (hypometabolic zone) were regarded as positive. The PET and PET z-score maps were both considered to determine the patient's laterality.

## Statistical analysis

### Quantitative whole brain metabolic alteration analysis

The mean values of NAA/Cr were calculated for selected ROIs. Additionally, the asymmetry indices (AIs) were also calculated for each pair of bilateral ROIs with the following formula:  $AI = (L - R) / (L + R)$ .

The two-tailed Wilcoxon signed-rank tests were applied to compare the metabolic ratios between the ipsilateral and contralateral ROIs in mTLE group. The two-tailed Wilcoxon rank-sum tests were used for group comparisons. False discovery rate (FDR) was used to correct for multiple comparisons, and the *P* value below 0.05 was considered statistically significant.

### Feature importance evaluation and classification for lateralization of mTLE

The AIs of NAA/Cr and FDG SUVR in hippocampus, amygdala, superior temporal gyrus, thalamus, and insula were extracted as features for lateralization of MRI-negative mTLE. The importance of these features in lateralization was evaluated and ranked by calculating the Fisher score, a commonly supervised feature selection technique [49]. A higher Fisher score indicates that the feature is more informative in lateralization. Subsequently, the hippocampal NAA/Cr, FDG SUVR, and top five features were added into the logistic regression model for lateralization. In the classification models, MRI-negative left mTLE (LTLE) and right mTLE (RTLE) were defined as positive and negative samples respectively. Due to the limited sample sizes, a leave-one-out cross-validation strategy was implemented to corroborate the predictive generalizability of models. The area under the curve (AUC) of receiver operating characteristic (ROC) curve was calculated to evaluate the performance of each regression model. The critical brain regions were identified as the ROI combination with the best diagnostic performance (the highest AUC of the ROC).

### Hierarchical moderated multiple regression analysis

To further elucidate the relationship of NAA/Cr and FDG SUVR, we performed targeted analyses in the hippocampus of mTLE. Coupling between changes of  $AI_{NAA}$  and  $AI_{FDG}$  in the hippocampus was evaluated by Pearson's correlations. To understand how disease (i.e., epilepsy duration since onset) impacts the relationship between  $AI_{NAA}$  and  $AI_{FDG}$ ,

we applied the hierarchical moderated multiple regression [50]. To evaluate the moderating effect, we sequentially entered  $AI_{NAA}$ , epilepsy duration and the interaction term as 'epilepsy duration  $\times$   $AI_{NAA}$ ' to a regression model to predict  $AI_{FDG}$  as a response variable. In a separate model,  $AI_{FDG}$ , epilepsy duration, and interaction term as 'epilepsy duration  $\times$   $AI_{FDG}$ ' were entered to predict  $AI_{NAA}$ . We tested whether adding the interaction term increased the variance explained by the model in successive regression steps ( $\Delta R^2$ , according to the available guidelines [51]). To control for confounds, gender and age were entered as nuisance variables. To interpret the moderating effects, we plotted simple slopes of significant interactions for the relationship between  $AI_{NAA}$  and the  $AI_{FDG}$  when the levels of the moderator variable (epilepsy duration) were one standard deviation above and below the mean. Similarly, we evaluated the moderating effect of brain region atrophy (defined as  $ROI_{atrophy} = (Volume_{ROI_{contral}} - Volume_{ROI_{ipsi}}) / Volume_{ROI_{contral}}$ ).

## Results

### Patient demographics

The patient demographics and clinical information are provided in Table 1 and Supplementary Table 2, showing 48 patients diagnosed with unilateral mTLE (22 right, 26 left, male/female 31/17, age range 10–58 years). For comparisons, age- and sex-matched healthy controls (male/female 19/17, age range 21–43 years) were included (sex, *P* = 0.275; age, *P* = 0.674).

### MRSI derived metabolic maps detect changes in epileptogenic zones

Representative whole-brain MRSI maps acquired from a patient with unilateral hippocampal sclerosis (HS) and the corresponding routine MRI images and [ $^{18}$ F]FDG PET images are shown in Fig. 2. Visually decreased NAA in the left hippocampus as well as the left temporal lobe is readily observed, consistent with hypometabolism in [ $^{18}$ F]FDG PET. Increased mIn in left hippocampus is observed, consistent with the hyperintensity in T2 FLAIR image. Spectra of ipsilateral and contralateral hippocampi also show decreased NAA and increased mIn.

Four representative MRI-negative cases, where routine MRIs are inconclusive, are shown in Fig. 3. The NAA changes are visualized in the z-score maps in coronal views, and the clusters of suspicious lesions with decreased NAA/Cr are highlighted. The NAA/Cr reductions in the first three cases are shown around hippocampus (patient #7), hippocampus-thalamus (patient #11), and the amygdala (patient #30), which are in accordance with the FDG



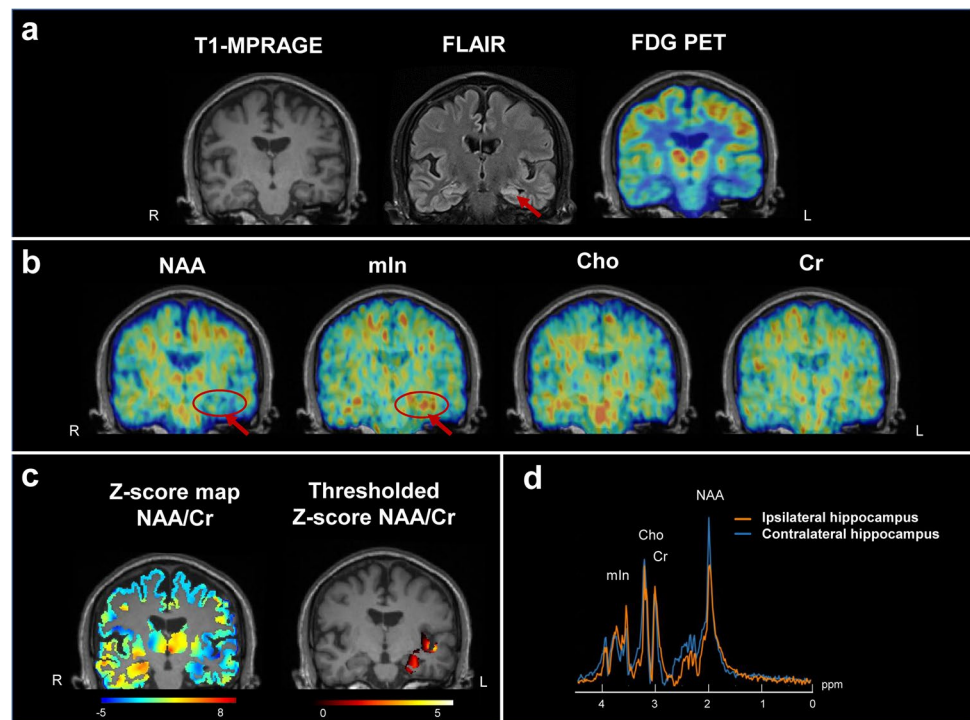
**Table 1** Demographics and clinical information of participants

	mTLE	HC	<i>P</i> value
Number of subjects	48	36	
Sex (male/female)	31/17	19/17	0.275 <sup>a</sup>
Age at evaluation (year), median (range)	24 (10–58)	26 (21–43)	0.674 <sup>b</sup>
Age at seizure onset (year), median (range)	15 (1–47)		
Disease duration (year), median (range)	10 (1–43)		
Seizure frequency (per year), median (range)	15 (1–300)		
Number of patients with SEEG evaluations and had surgery	34		
Postsurgical outcome Engel Class <sup>c</sup> (I/II–IV)/Miss	22/11/1		

<sup>a)</sup> Chi-square test; <sup>b)</sup> Two-sample t test. <sup>c)</sup> Postsurgical seizure outcome was assessed using the Engel post-operative outcome scale (Engel, 1993)

HC, healthy control; mTLE, mesial temporal lobe epilepsy; SEEG, stereoelectroencephalography

**Fig. 2** Multimodal images from the representative MR-positive left hippocampal sclerosis case #24. **a** The T1-weighted image, T2 FLAIR, [<sup>18</sup>F]FDG PET, and **b** MRSI maps including NAA, Cr, Cho, and mIn are displayed in coronal views. Decreased NAA and increased mIn in left hippocampus are observed. All images were registered to the structural T1-weighted image. **c** Z-score maps corresponding to the NAA/Cr were masked to highlight the gray matter. To identify the suspicious lesion, the z-score NAA/Cr maps were thresholded using the z-score < -1 and a minimum cluster size of  $k > 40$ . **d** Spectra of ipsilateral vs. contralateral hippocampus



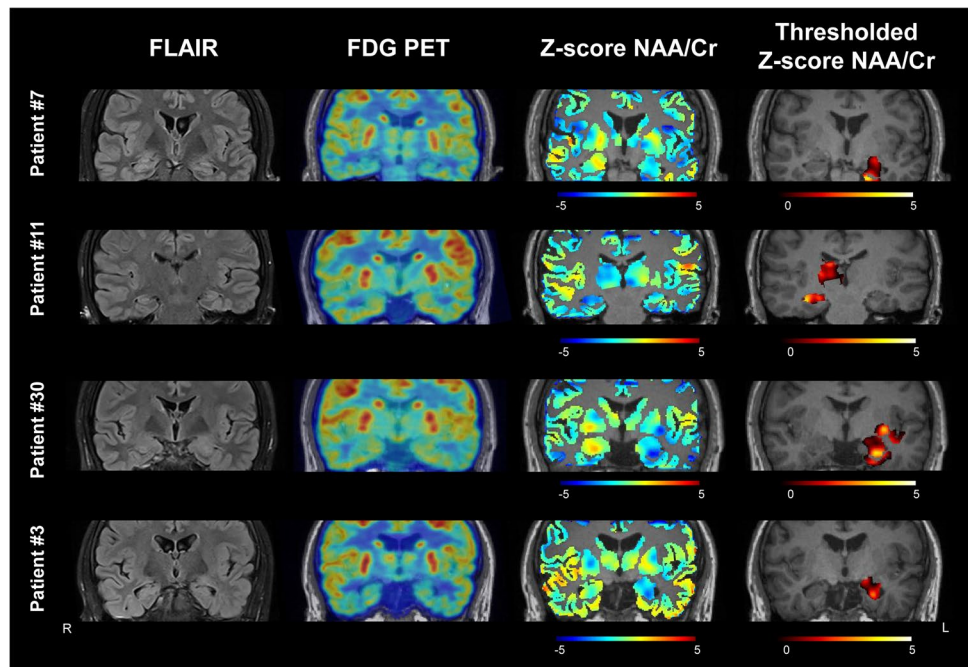
hypometabolism. In another case (patient #3) with normal [<sup>18</sup>F]FDG PET, the suspicious lesions with NAA decrease are readily observable in the left hippocampus, which was confirmed by presurgical intracranial SEEG.

### [<sup>18</sup>F]FDG PET and NAA map are complementary in visual assessment

The detection rate of routine MRI is 25 out of 48 (52.1%; 95% confidence interval: 38.3%, 65.5%). NAA maps showed improvement in diagnostic accuracy by detecting 41 out of 48 (85.4%; 95% confidence interval: 72.8%, 92.8%), a performance equivalent to that of [<sup>18</sup>F]FDG PET (85.4%; 95% confidence interval: 72.8%, 92.8%). Combined NAA maps

and [<sup>18</sup>F]FDG PET correctly lateralized 44 out of 48 mTLE (91.7%; 95% confidence interval: 80.5%, 96.7%). We then divided mTLE patients into six subgroups (MRI-HS, MRI-negative, FDG-positive, FDG-negative, NAA-positive, NAA-negative) according to visual assessment and whether lesions were identifiable. Figure 4 shows the crossovers between the subgroups. Among the 23 MRI-negative patients, 18 were lateralized based on NAA maps, while three out of five remaining MRI-negative cases were clearly lateralized by [<sup>18</sup>F]FDG PET. On the other hand, [<sup>18</sup>F]FDG PET alone correctly lateralized 17/23 MRI negative cases, while four out of six MRI-negative PET-negative cases were clearly lateralized in NAA maps. Individual diagnosis results are summarized in Supplementary Table 2.

**Fig. 3** Multimodal images from representative cases with MRI-negative mTLE. FLAIR, [<sup>18</sup>F]FDG PET, z-score maps of NAA/Cr, and thresholded z-score maps of NAA/Cr from MRI-negative PET-positive mTLE cases #7 (Left mTLE), #11 (Right mTLE), #30 (Left mTLE), and MRI-negative PET-negative case #3 (Left mTLE). All images were registered to the structural T1-weighted images. The z-score maps corresponding to the NAA/Cr were masked to highlight the gray matter. To identify the suspicious lesions, z-score NAA/Cr maps were thresholded using the z-score < -1 and a minimum cluster size of k > 40

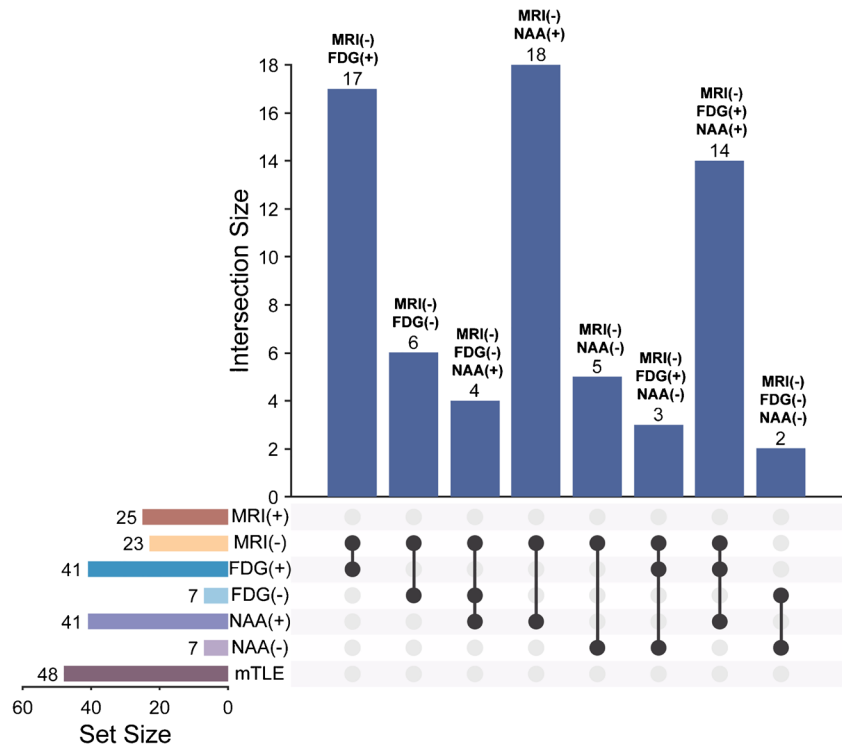


**Widespread metabolic alterations in mTLE**

Overall NAA/Cr changes are shown in Fig. 5 and Supplementary Table 3 for MRI-HS and MRI-negative mTLE. MRI-HS (Fig. 5a) and MRI-negative mTLE (Fig. 5b) exhibited significant NAA decrease in the ipsilateral hippocampi and amygdala compared to HC (MRI-HS:  $P_{FDR} < 0.001$  for hippocampus,  $P_{FDR} < 0.001$  for amygdala; MRI-negative:

$P_{FDR} < 0.001$  for hippocampus,  $P_{FDR} < 0.001$  for amygdala). Extrahippocampal NAA/Cr reduction of all mTLE was found in widespread regions (Supplementary Table 3). Notably, thalamus, superior temporal gyrus, fusiform, transverse temporal cortex, and insula show significant NAA/Cr reduction in both ipsilateral and contralateral sides of the MRI-HS group, while only show NAA/Cr reduction in the ipsilateral side of the MRI-negative group, compared to HC.

**Fig. 4** Upset diagram showing the results of the visual assessment. The horizontal bar chart shows the count of each subgroup among mTLE patients. The black dots and connecting lines indicate crossover among subgroups; The counts of each crossover combo are shown on the top of vertical bars. The (+) symbol indicates that the corresponding modality has succeeded in lateralizing the epileptogenic zone, whereas the (-) symbol denotes failure. For example, in the leftmost bar, 17 patients were identified as MRI(-) but FDG(+)



Among the pairwise comparisons between NAA/Cr of ipsilateral and contralateral ROIs, the ipsilateral hippocampus ( $P_{\text{FDR}} = 0.029$ ), amygdala ( $P_{\text{FDR}} = 0.026$ ) and superior temporal gyrus ( $P_{\text{FDR}} = 0.026$ ) of MRI-HS had significantly lower NAA/Cr compared to the contralateral ROIs (Fig. 5c). For MRI-negative patients, decreased NAA/Cr were significant in hippocampus ( $P_{\text{FDR}} = 0.041$ ), thalamus ( $P_{\text{FDR}} = 0.048$ ), amygdala ( $P_{\text{FDR}} = 0.041$ ), and insula ( $P_{\text{FDR}} = 0.048$ ) (Fig. 5d). In addition, the ipsilateral hippocampal of MRI-HS mTLE showed significantly higher mIn/Cr compared with contralateral hippocampus. No statistically significant differences of mIn/Cr were found in other ROIs, or in Cho/Cr (Supplementary Fig. 3).

### Combined asymmetry indices of NAA/Cr and FDG uptake improve MRI-negative mTLE lateralization

The asymmetry indices (AI) of NAA/Cr and FDG SUVR between ipsilateral and contralateral hippocampus, amygdala, superior temporal gyrus, thalamus, and insula were used to automate lateralization of MRI-negative mTLE.

Importance of features are ranked by Fisher score (Fig. 6a). The AIs of FDG SUVR in hippocampus and thalamus, NAA/Cr in amygdala, insula, and thalamus are ranked top five.

Logistic regression models were used to evaluate the performance of NAA, FDG, and NAA+FDG in lateralizing MRI-negative mTLE patients. The combination of hippocampal NAA+FDG reached a higher AUC of 0.856, than hippocampal FDG (AUC = 0.811) or hippocampal NAA/Cr (AUC = 0.697). The top five features together obtained the best performance with the highest AUC of 0.939 (Fig. 6b). At the best operating point, 91.3% (21/23) of MRI-negative cases were accurately lateralized using the best model (Fig. 6c).

### The moderator effect of disease duration and hippocampal atrophy on the coupling between NAA and FDG

In hippocampus, we found significant associations between  $AI_{\text{NAA}}$  and  $AI_{\text{FDG}}$  ( $r = 0.46$ ,  $P = 0.001$ ) (Fig. 7a). Hierarchical moderated multiple regression analysis revealed

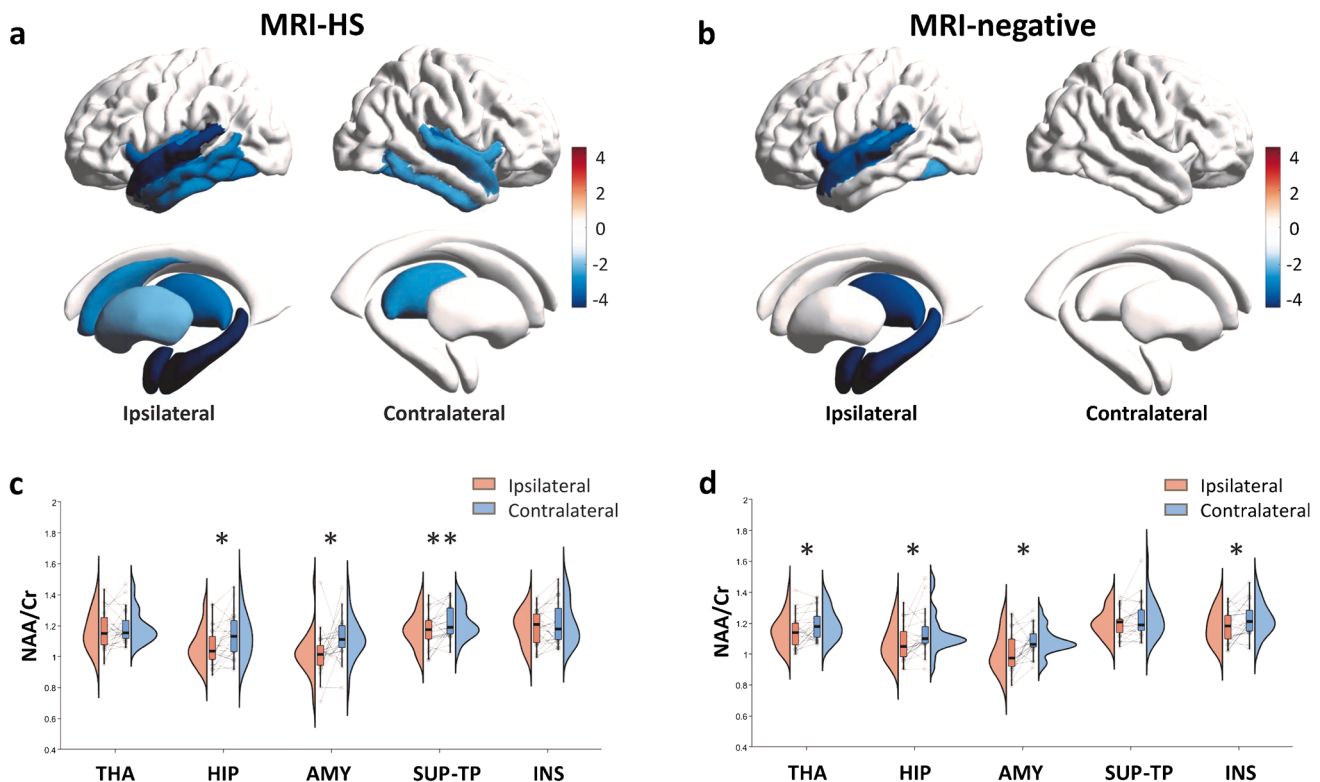


**Fig. 5** Metabolic patterns of NAA/Cr in MRI-HS and MRI-negative mTLE patients. Significant NAA/Cr alteration in MRI-HS **a** and MRI-negative **b** mTLE patients in comparison to healthy controls. ROIs are colored according to their corresponding z-statistics of Wilcoxon rank-sum tests. Pairwise comparisons of NAA/Cr in the ipsilateral thalamus, hippocampus, amygdala, superior temporal gyrus and

insula in MRI-HS **c** and MRI-negative mTLE patients **d** to NAA/Cr in the contralateral ROIs. Each patient's values are connected by solid line. Wilcoxon signed-rank tests are used.  $*P_{\text{FDR}} < 0.05$ , corrected by FDR. AMY, amygdala; HIP, hippocampus; INS, insula; SUP-TP, superior temporal gyrus; THA, thalamus



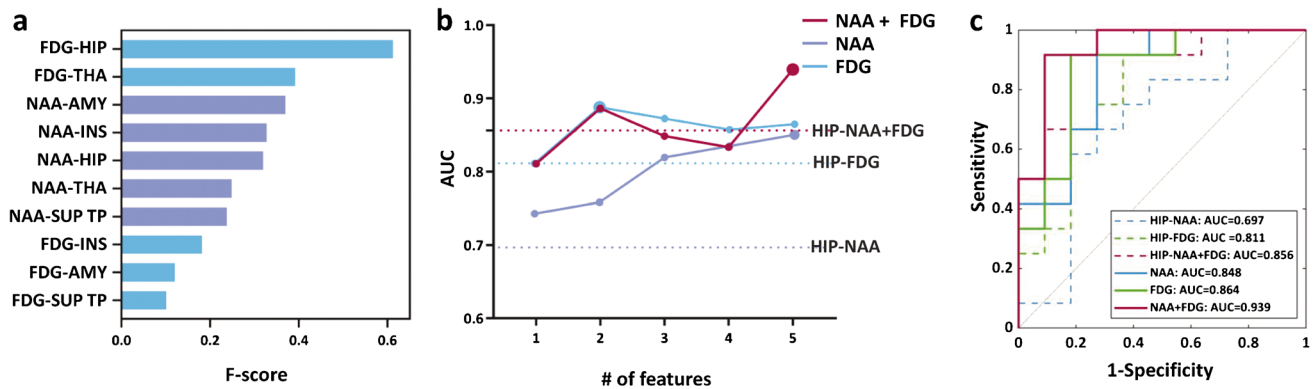


**Fig. 6** Lateralization of MRI-negative mTLE using single or combined metabolic features. **a** Bar plot of feature importance of Fisher scores on selected features. **b** The AUC of the hippocampal NAA/Cr, FDG PET, and top  $n$  ( $n = 1$  to  $5$ ) most important features of NAA, FDG, and NAA+FDG combination for lateralization. **c** The ROC

curves demonstrate the performance of the classification models. AMY, amygdala; AUC, area under the curve; HIP, hippocampus; INS, insula; ROC, receiver operating characteristic; SUP-TP, superior temporal gyrus; THA, thalamus

significant two-way interactions between ‘epilepsy duration  $\times$   $AI_{NAA}$ ’ in the hippocampus that predicted changes in  $AI_{FDG}$  ( $P = 0.002$ ) (Fig. 7b), while no significant interactions were found in ‘epilepsy duration  $\times$   $AI_{FDG}$ ’ that predict changes in  $AI_{NAA}$  ( $P = 0.851$ ), indicating that epilepsy duration moderates the associations between  $AI_{NAA}$  and  $AI_{FDG}$ . Specifically, the conditional effect of  $AI_{NAA}$  on predicting  $AI_{FDG}$  was high ( $\beta = 1.291$ ,  $P < 0.001$ ) at longer epilepsy durations ( $> 22$  years, 1 SD above the mean), moderate ( $\beta = 0.762$ ,  $P < 0.001$ ) at medium epilepsy duration, but not significant ( $\beta = 0.233$ ,  $P = 0.343$ ) at short epilepsy durations ( $\leq 2$  years, 1 SD below the mean), which indicated that longer epilepsy duration led to higher slope when predicting  $AI_{FDG}$  using  $AI_{NAA}$ . Additionally, we observed significant moderation effects of hippocampal atrophy on the predictive relationship of  $AI_{NAA}$  to  $AI_{FDG}$  ( $P = 0.007$ ), while severer atrophy corresponds to higher slope (Fig. 7c).

## Discussion

This pilot study shows the remarkable efficacy of simultaneous 3D whole brain MRSI and [ $^{18}$ F]FDG PET imaging in a clinical setting and its potential benefits to the diagnosis of MRI-negative mTLE. Further, this study pioneers the simultaneous mapping of NAA levels and FDG uptake in hippocampal sclerosis. Remarkably, the data acquisition of SPICE is user-friendly and operator independent. High-quality whole-brain MRSI was made possible by several key features of SPICE technology: (1) built-in capability for water referencing; (2) motion correction; (3) detection and correction of magnetic field inhomogeneity and drift; and (4) denoising capability. We obtained 3D maps of NAA, mIn, and Cho concurrently at a nominal spatial resolution

of  $2.0 \times 3.1 \times 2.7$  mm<sup>3</sup> or  $2.0 \times 3.1 \times 3.8$  mm<sup>3</sup> of epilepsy patients in 9–12 min, within a clinically acceptable time.

In this study, we correctly lateralized 85.4% (41/48) of mTLE patients using NAA-to-Cr ratio, surpassing 52.1% (25/48) using routine MRI in visual assessment. Adding FDG hypometabolism further enhanced the lateralization accuracy to 91.7% (44/48). Integrating both MRSI and [ $^{18}$ F]FDG PET into logistic models, MRI-negative mTLE lateralization accuracy reached 91.3%. A recent worldwide ENIGMA-epilepsy study employing artificial intelligence and ROI-level diffusion MRI demonstrated accuracy rates of 53–62% for non-lesional patients in the lateralization of mTLE in an assembled cohort of 275 patients [52]. The study highlights the potential of neurometabolic mapping in visualizing MRI-unidentifiable lesions, thus improving presurgical evaluations for mTLE.

Previously, despite many observations of metabolic profile changes in the mesial temporal brain area using MRS, only a few have discussed any specific ROIs beyond the hippocampus, such as the decrease of NAA in thalamus [26, 53], insula [29], and the overall brain tissue [54]. Enabled by high-resolution whole-brain mapping of SPICE, we systematically explored the metabolic changes within the epileptogenic network of mTLE, and found widespread regional NAA/Cr reduction in the hippocampus, amygdala, thalamus, and insula, and superior temporal gyrus, which can provide valuable information for lateralization. Especially for MRI-negative cases, the NAA/Cr in amygdala and thalamus were ranked higher in feature importance compared to hippocampal NAA/Cr, while they appeared normal on T2 FLAIR images. The observed NAA decrease are in line with evidence supporting neuronal damage progressively expanding from the hippocampus to the limbic structure and thalamus during the epileptogenesis by electrophysiological study [55,

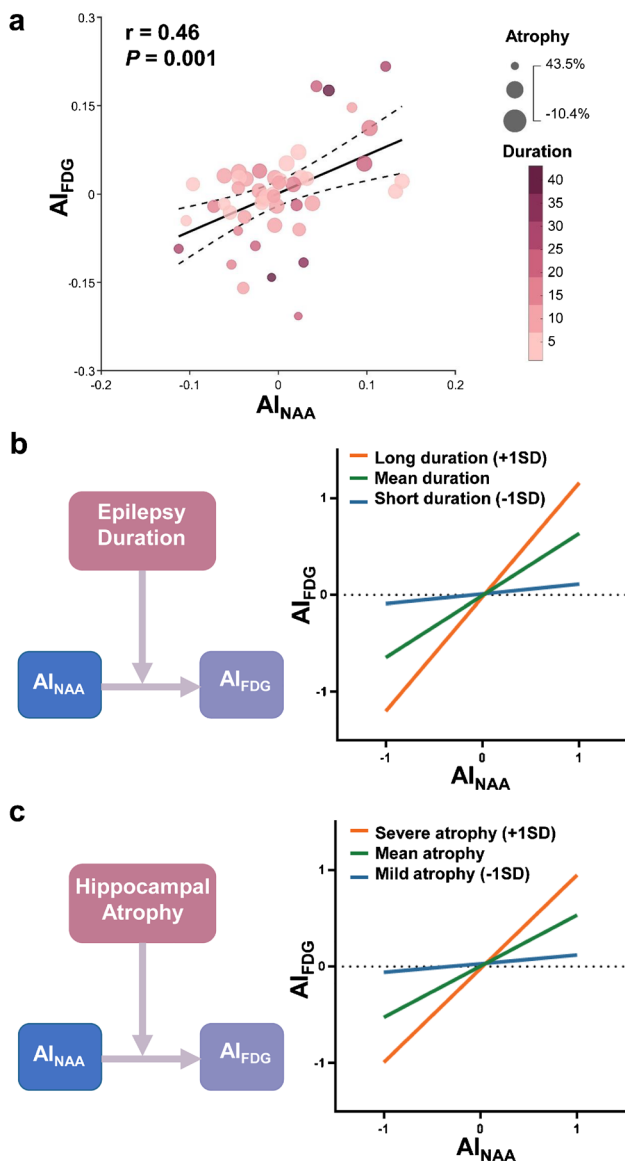


**Fig. 7** Moderator effects of disease duration and hippocampal atrophy on the couplings between  $AI_{NAA}$  and  $AI_{FDG}$ . **a** The scatter plot illustrates the correlation between these two measures in the hippocampus. Panels **b** and **c** demonstrate the moderator effects of epilepsy duration and hippocampal atrophy, respectively, on the coupling between hippocampal  $AI_{NAA}$  and  $AI_{FDG}$ . The left side of each panel depicts a schematic of the moderator model, while the right side shows the relationship between  $AI_{NAA}$  and  $AI_{FDG}$  at three fixed moderator levels (mean, mean + 1 SD, mean - 1 SD)

56], and animal models [9, 57]. Cortical NAA decrease also aligns with glucose hypometabolism detected by [ $^{18}F$ ]FDG PET in the insula, superior temporal gyrus [58], and extra-hippocampal gray matter atrophy indicated by voxel-based morphometry [59, 60]. These findings highlight that high-resolution whole-brain MRSI has the potential to characterize comprehensive metabolic changes in the epileptogenic network.

Research with hybrid [ $^{18}F$ ]FDG PET/MR system has been conducted in epilepsy patients. Most of them focus on fusion of FDG with high-resolution anatomical MR images [61, 62], with emerging investigations on the synergy between FDG and MRI-based morphometric [63], functional [64, 65], microstructure [58], relaxometry [66], and perfusion markers [67]. Hybrid PET/MRI system facilitates identically controlled physiological condition: awake, resting state, fast, for both modalities. Given possible physiological driven fluctuations in glucose uptake [32, 34] and NAA [33] at varying hours or days, this setup presents a unique opportunity to explore the concurrent pathophysiological status of NAA and glucose uptake, bolstering the reliability of findings. To our knowledge, this study is the first simultaneous PET/MRSI attempt to investigate the concurrent metabolic alterations associated with epileptogenesis in mTLE.

As a unique and abundant neuronal metabolite, NAA has potential to specifically reflect neuronal mitochondrial dysfunction in epileptic brain [68, 69]. On the other hand, interictal cerebral glucose uptake is also considered to be driven by oxidative neuronal metabolism which primarily takes place in the mitochondria. In this study, we found the association between NAA and FDG in hippocampus was moderated by epilepsy disease duration. The longer epilepsy durations correspond to higher correlation coefficient ( $\beta = 1.291$ ) of NAA predicting glucose metabolism. At short disease duration, the decoupling between NAA level and glucose uptake may indicate divergent underlying mechanisms. In such instances, reduced NAA may result from its role as a glutamate reservoir [70], or as acetyl-CoA reservoir upon oxidative stress [68], while FDG uptake might appear normal potentially due to the subsequent activation of glia cells upon neuronal stress [9, 71]. As the disease progresses, cumulative seizure-induced damage to the glial-neuronal unit may strengthen the relationship between NAA and [ $^{18}F$ ]FDG PET. Severe atrophy also exhibit similar moderation effects, which may suggest when neuronal loss dominate neuropathology of HS, NAA level and FDG uptake converge on reflecting the same process. Collectively, these findings support the progressive nature of mTLE, where repeated seizures contribute to the worsening of neuropathology. Note that, only NAA reduction showed very high sensitivity at short disease duration, which indicated its unique clinical value as a highly sensitive imaging marker for patients at a relatively early stage of the disease.

This study has limitations. Firstly, our cohort comprised a relatively small sample size of 48 mTLE patients, which necessitated the utilization of leave-one-out cross-validation for testing the classification models. Future studies with larger-scale cohorts are warranted to fully explore the potential of whole-brain high-resolution metabolic mapping, and to quantify the variability of the metabolic alteration profiles across the full range of clinical presentations, including

different types of epileptic lesions. Secondly, we only focused on gray matter NAA in this study. Given the role of NAA in myelination and previous findings on possible demyelination in mTLE, investigations in white matter NAA would be worthwhile. Further improvements and investigations could help clinical usage, especially in the following aspects: (1) Advanced feature generation or machine learning approaches may further enhance the classification performance. (2) More subtle neuronal metabolites and neurotransmitters such as Glu, Gln, and GABA could be obtained at higher magnetic field strength (e.g., 7 T) and/or with technical improvements. Simultaneous mapping of their concentration changes may shed lights in better understanding and characterization of epileptogenic network and treatment response.

## Conclusion

In conclusion, these findings highlight MRSI's potential added value in the precise lateralization of mTLE, both as part of MRI examination protocol on a stand-alone MRI and in combination with [<sup>18</sup>F]FDG PET. Concurrent associations between glucose uptake and NAA level are moderated by disease progression of epilepsy.

**Supplementary Information** The online version contains supplementary material available at <https://doi.org/10.1007/s00259-023-06465-0>.

**Funding** The study was partially supported by the National Natural Science Foundation of China (No. 62101321, and No. 82372073), Shanghai Municipal Health Commission (No. 202240031), and Shanghai Municipal Key Clinical Specialty (shslczdzk03403).

**Data Availability** The data that support the findings of this study are available upon request from the corresponding author, J.L.

## Declarations

**Ethical approval** This study was performed in line with the principles of the Declaration of Helsinki. Approval was granted by the Ethics Committee of Ruijin hospital (Approved No. 2016-128).

**Consent to participate** Informed consent was obtained from all individual participants included in the study.

**Conflict of interest** The authors declare no competing interests.

## References

- Thijs RD, Surges R, O'Brien TJ, Sander JW. Epilepsy in adults. *Lancet*. 2019;393:689–701. [https://doi.org/10.1016/s0140-6736\(18\)32596-0](https://doi.org/10.1016/s0140-6736(18)32596-0).
- Engel J Jr, McDermott MP, Wiebe S, Langfitt JT, Stern JM, Dewar S, et al. Early surgical therapy for drug-resistant temporal lobe epilepsy: a randomized trial. *Jama*. 2012;307:922–30. <https://doi.org/10.1001/jama.2012.220>.
- Thom M. Review: Hippocampal sclerosis in epilepsy: a neuropathology review. *Neuropathol Appl Neurobiol*. 2014;40:520–43. <https://doi.org/10.1111/nan.12150>.
- Blümcke I, Thom M, Aronica E, Armstrong DD, Bartolomei F, Bernardoni A, et al. International consensus classification of hippocampal sclerosis in temporal lobe epilepsy: a Task Force report from the ILAE Commission on Diagnostic Methods. *Epilepsia*. 2013;54:1315–29. <https://doi.org/10.1111/epi.12220>.
- Muhlhofer W, Tan YL, Mueller SG, Knowlton R. MRI-negative temporal lobe epilepsy-what do we know? *Epilepsia*. 2017;58:727–42. <https://doi.org/10.1111/epi.13699>.
- Tellez-Zenteno JF, Hernandez Ronquillo L, Moien-Afshari F, Wiebe S. Surgical outcomes in lesional and non-lesional epilepsies: a systematic review and meta-analysis. *Epilepsy Res*. 2010;89:310–8. <https://doi.org/10.1016/j.epilepsyres.2010.02.007>.
- Duncan JS, Winston GP, Koepp MJ, Ourselin S. Brain imaging in the assessment for epilepsy surgery. *The Lancet Neurology*. 2016;15:420–33. [https://doi.org/10.1016/s1474-4422\(15\)00383-x](https://doi.org/10.1016/s1474-4422(15)00383-x).
- Lagarde S, Boucekine M, McGonigal A, Carron R, Scavarda D, Trebuchon A, et al. Relationship between PET metabolism and SEEG epileptogenicity in focal lesional epilepsy. *Eur J Nucl Med Mol Imaging*. 2020;47:3130–42. <https://doi.org/10.1007/s00259-020-04791-1>.
- Lee EM, Park GY, Im KC, Kim ST, Woo CW, Chung JH, et al. Changes in glucose metabolism and metabolites during the epileptogenic process in the lithium-pilocarpine model of epilepsy. *Epilepsia*. 2012;53:860–9. <https://doi.org/10.1111/j.1528-1167.2012.03432.x>.
- Filibian M, Frasca A, Maggioni D, Micotti E, Vezzani A, Ravizza T. In vivo imaging of glia activation using 1H-magnetic resonance spectroscopy to detect putative biomarkers of tissue epileptogenicity. *Epilepsia*. 2012;53:1907–16. <https://doi.org/10.1111/j.1528-1167.2012.03685.x>.
- Reddy SD, Younus I, Sridhar V, Reddy DS. Neuroimaging biomarkers of experimental epileptogenesis and refractory epilepsy. *Int J Mol Sci*. 2019;20(1):220. <https://doi.org/10.3390/ijms20010220>.
- Doelken MT, Stefan H, Pauli E, Stadlbauer A, Struffert T, Engelhorn T, et al. (1)H-MRS profile in MRI positive- versus MRI negative patients with temporal lobe epilepsy. *Seizure*. 2008;17:490–7. <https://doi.org/10.1016/j.seizure.2008.01.008>.
- Rho JM, Boison D. The metabolic basis of epilepsy. *Nat Rev Neurol*. 2022;18:333–47. <https://doi.org/10.1038/s41582-022-00651-8>.
- Carne RP, O'Brien TJ, Kilpatrick CJ, MacGregor LR, Hicks RJ, Murphy MA, et al. MRI-negative PET-positive temporal lobe epilepsy: a distinct surgically remediable syndrome. *Brain*. 2004;127:2276–85. <https://doi.org/10.1093/brain/awh257>.
- LoPinto-Khoury C, Sperling MR, Skidmore C, Nei M, Evans J, Sharan A, et al. Surgical outcome in PET-positive, MRI-negative patients with temporal lobe epilepsy. *Epilepsia*. 2012;53:342–8. <https://doi.org/10.1111/j.1528-1167.2011.03359.x>.
- Niu N, Xing H, Wu M, Ma Y, Liu Y, Ba J, et al. Performance of PET imaging for the localization of epileptogenic zone in patients with epilepsy: a meta-analysis. *Eur Radiol*. 2021. <https://doi.org/10.1007/s00330-020-07645-4>.
- Oz G, Alger JR, Barker PB, Bartha R, Bizzi A, Boesch C, et al. Clinical proton MR spectroscopy in central nervous system disorders. *Radiology*. 2014;270:658–79. <https://doi.org/10.1148/radiol.13130531>.
- Pan JW, Kuzniecky RI. Utility of magnetic resonance spectroscopic imaging for human epilepsy. *Quant Imaging Med Surg*. 2015;5:313–22. <https://doi.org/10.3978/j.issn.2223-4292.2015.01.03>.
- Pan JW, Williamson A, Cavus I, Hetherington HP, Zaveri H, Petroff OA, et al. Neurometabolism in human epilepsy. *Epilepsia*. 2008;49(Suppl 3):31–41. <https://doi.org/10.1111/j.1528-1167.2008.01508.x>.

20. Fernández-Vega N, Ramos-Rodríguez JR, Alfaro F, Barbancho M, García-Casares N. Usefulness of magnetic resonance spectroscopy in mesial temporal sclerosis: a systematic review. *Neuroradiology*. 2021;63:1395–405. <https://doi.org/10.1007/s00234-021-02704-z>.
21. Vermathen P, Ende G, Laxer KD, Knowlton RC, Matson GB, Weiner MW. Hippocampal N-acetylaspartate in neocortical epilepsy and mesial temporal lobe epilepsy. *Ann Neurol*. 1997;42:194–9. <https://doi.org/10.1002/ana.410420210>.
22. Petroff OA, Errante LD, Kim JH, Spencer DD. N-acetyl-aspartate, total creatine, and myo-inositol in the epileptogenic human hippocampus. *Neurology*. 2003;60:1646–51. <https://doi.org/10.1212/01.wnl.0000068020.85450.8b>.
23. Cendes F, Andermann F, Preul MC, Arnold DL. Lateralization of temporal lobe epilepsy based on regional metabolic abnormalities in proton magnetic resonance spectroscopic images. *Ann Neurol*. 1994;35:211–6. <https://doi.org/10.1002/ana.410350213>.
24. Connelly A, Van Paesschen W, Porter DA, Johnson CL, Duncan JS, Gadian DG. Proton magnetic resonance spectroscopy in MRI-negative temporal lobe epilepsy. *Neurology*. 1998;51:61–6. <https://doi.org/10.1212/wnl.51.1.61>.
25. Hetherington HP, Kuzniecky RI, Vives K, Devinsky O, Pacia S, Luciano D, et al. A subcortical network of dysfunction in TLE measured by magnetic resonance spectroscopy. *Neurology*. 2007;69:2256–65. <https://doi.org/10.1212/01.wnl.0000286945.21270.6d>.
26. Pan JW, Duckrow RB, Gerrard J, Ong C, Hirsch LJ, Resor SR Jr, et al. 7T MR spectroscopic imaging in the localization of surgical epilepsy. *Epilepsia*. 2013;54:1668–78. <https://doi.org/10.1111/epi.12322>.
27. Mueller SG, Laxer KD, Cashdollar N, Flenniken DL, Matson GB, Weiner MW. Identification of abnormal neuronal metabolism outside the seizure focus in temporal lobe epilepsy. *Epilepsia*. 2004;45:355–66. <https://doi.org/10.1111/j.0013-9580.2004.27603.x>.
28. Tan Q, Sun H, Wang W, Wu X, Hao N, Su X, et al. Quantitative MR spectroscopy reveals metabolic changes in the dorso-lateral prefrontal cortex of patients with temporal lobe epilepsy. *Eur Radiol*. 2018;28:4496–503. <https://doi.org/10.1007/s00330-018-5443-x>.
29. Capizzano AA, Vermathen P, Laxer KD, Matson GB, Maudsley AA, Soher BJ, et al. Multisection proton MR spectroscopy for mesial temporal lobe epilepsy. *AJNR Am J Neuroradiol*. 2002;23:1359–68.
30. Spencer DD, Gerrard JL, Zaveri HP. The roles of surgery and technology in understanding focal epilepsy and its comorbidities. *Lancet Neurol*. 2018;17:373–82. [https://doi.org/10.1016/s1474-4422\(18\)30031-0](https://doi.org/10.1016/s1474-4422(18)30031-0).
31. Zijlmans M, Zweiphenning W, van Klink N. Changing concepts in presurgical assessment for epilepsy surgery. *Nat Rev Neurol*. 2019;15:594–606. <https://doi.org/10.1038/s41582-019-0224-y>.
32. van der Veen DR, Shao J, Chapman S, Leevy WM, Duffield GE. A 24-hour temporal profile of in vivo brain and heart pet imaging reveals a nocturnal peak in brain 18F-fluorodeoxyglucose uptake. *PLoS One*. 2012;7:e31792. <https://doi.org/10.1371/journal.pone.0031792>.
33. Soreni N, Noseworthy MD, Cormier T, Oakden WK, Bells S, Schachar R. Intra-individual variability of striatal (1)H-MRS brain metabolite measurements at 3 T. *Magn Reson Imaging*. 2006;24:187–94. <https://doi.org/10.1016/j.mri.2005.10.027>.
34. Boellaard R. Standards for PET image acquisition and quantitative data analysis. *J Nucl Med*. 2009;50(Suppl 1):11s–20s. <https://doi.org/10.2967/jnumed.108.057182>.
35. Lam F, Liang Z-PA. subspace approach to high-resolution spectroscopic imaging. *Magn Reson Med*. 2014;71:1349–57. <https://doi.org/10.1002/mrm.25168>.
36. Ma C, Lam F, Ning Q, Johnson CL, Liang Z-P. High-resolution (1) H-MRSI of the brain using short-TE SPICE. *Magn Reson Med*. 2017;77:467–79. <https://doi.org/10.1002/mrm.26130>.
37. Li Y, Lam F, Clifford B, Liang Z-PA. subspace approach to spectral quantification for MR spectroscopic imaging. *IEEE Trans Biomed Eng*. 2017;64:2486–9. <https://doi.org/10.1109/tbme.2017.2741922>.
38. Guo R, Zhao Y, Li Y, Li Y, Liang Z-P. Simultaneous metabolic and functional imaging of the brain using SPICE. *Magn Reson Med*. 2019;82:1993–2002. <https://doi.org/10.1002/mrm.27865>.
39. Peng X, Lam F, Li Y, Clifford B, Liang Z-P. Simultaneous QSM and metabolic imaging of the brain using SPICE. *Magn Reson Med*. 2018;79:13–21. <https://doi.org/10.1002/mrm.26972>.
40. Li Y, Wang T, Zhang T, Lin Z, Li Y, Guo R, et al. Fast high-resolution metabolic imaging of acute stroke with 3D magnetic resonance spectroscopy. *Brain*. 2020;143:3225–33. <https://doi.org/10.1093/brain/awaa264>.
41. Lin Z, Meng Z, Wang T, Guo R, Zhao Y, Li Y, et al. Predicting the onset of ischemic stroke with fast high-resolution 3D MR Spectroscopic Imaging. *J Magn Reson Imaging*. 2023. <https://doi.org/10.1002/jmri.28596>.
42. Guo R, Ma C, Li Y, Zhao Y, Wang T, Li Y, et al. High-resolution label-free molecular imaging of brain tumor. *Annu Int Conf IEEE Eng Med Biol Soc*. 2021;2021:3049–52. <https://doi.org/10.1109/embc46164.2021.9630623>.
43. Lam F, Ma C, Clifford B, Johnson CL, Liang Z-P. High-resolution (1) H-MRSI of the brain using SPICE: data acquisition and image reconstruction. *Magn Reson Med*. 2016;76:1059–70. <https://doi.org/10.1002/mrm.26019>.
44. Liang ZP. Spatiotemporal imaging with partially separable functions. 2007 4th IEEE international symposium on biomedical imaging: from nano to macro: IEEE; 2007; 988–91.
45. Lin A, Andronesi O, Bogner W, Choi IY, Coello E, Cudalbu C, et al. Minimum reporting standards for in vivo magnetic resonance spectroscopy (MRSinMRS): experts' consensus recommendations. *NMR Biomed*. 2021;34:e4484. <https://doi.org/10.1002/nbm.4484>.
46. Koesters T, Friedman KP, Fenchel M, Zhan Y, Hermosillo G, Babb J, et al. Dixon sequence with superimposed model-based bone compartment provides highly accurate PET/MR attenuation correction of the brain. *J Nucl Med*. 2016;57:918–24. <https://doi.org/10.2967/jnumed.115.166967>.
47. Presotto L, Ballarini T, Caminiti SP, Bettinardi V, Gianolli L, Perani D. Validation of (18)F-FDG-PET single-subject optimized SPM procedure with different PET scanners. *Neuroinformatics*. 2017;15:151–63. <https://doi.org/10.1007/s12021-016-9322-9>.
48. Spencer SS. Neural networks in human epilepsy: evidence of and implications for treatment. *Epilepsia*. 2002;43:219–27. <https://doi.org/10.1046/j.1528-1157.2002.26901.x>.
49. Gu Q, Li Z, Han J. Generalized fisher score for feature selection. *arXiv preprint arXiv:12023725*. 2012.
50. Aguinis H, Gottfredson RK. Best-practice recommendations for estimating interaction effects using moderated multiple regression. *J Organ Behav*. 2010;31:776–86. <https://doi.org/10.1002/job.686>.
51. Whisman MA, McClelland GH. Designing, testing, and interpreting interactions and moderator effects in family research. *J Fam Psychol*. 2005;19:111–20. <https://doi.org/10.1037/0893-3200.19.1.111>.
52. Gleichgerricht E, Munsell BC, Alhusaini S, Alvim MKM, Bargalló N, Bender B, et al. Artificial intelligence for classification of temporal lobe epilepsy with ROI-level MRI data: a worldwide ENIGMA-Epilepsy study. *Neuroimage Clin*. 2021;31:102765. <https://doi.org/10.1016/j.nicl.2021.102765>.
53. Pan JW, Spencer DD, Kuzniecky R, Duckrow RB, Hetherington H, Spencer SS. Metabolic networks in epilepsy by MR



- spectroscopic imaging. *Acta Neurol Scand.* 2012;126:411–20. <https://doi.org/10.1111/j.1600-0404.2012.01665.x>.
54. Kirov II, Kuzniecky R, Hetherington HP, Soher BJ, Davitz MS, Babb JS, et al. Whole brain neuronal abnormalities in focal epilepsy quantified with proton MR spectroscopy. *Epilepsy Res.* 2018;139:85–91. <https://doi.org/10.1016/j.eplepsyres.2017.11.017>.
  55. Amorim-Leite R, Remick M, Welch W, Abel TJ. History of the Network Approach in Epilepsy Surgery. *Neurosurg Clin N Am.* 2020;31:301–8. <https://doi.org/10.1016/j.nec.2020.03.011>.
  56. Bartolomei F, Chauvel P, Wendling F. Epileptogenicity of brain structures in human temporal lobe epilepsy: a quantified study from intracerebral EEG. *Brain.* 2008;131:1818–30. <https://doi.org/10.1093/brain/awn111>.
  57. Guo Y, Gao F, Wang S, Ding Y, Zhang H, Wang J, et al. In vivo mapping of temporospatial changes in glucose utilization in rat brain during epileptogenesis: an 18F-fluorodeoxyglucose-small animal positron emission tomography study. *Neuroscience.* 2009;162:972–9. <https://doi.org/10.1016/j.neuroscience.2009.05.041>.
  58. Aparicio J, Carreño M, Bargalló N, Setoain X, Rubí S, Rumià J, et al. Combined (18)F-FDG-PET and diffusion tensor imaging in mesial temporal lobe epilepsy with hippocampal sclerosis. *Neuroimage Clin.* 2016;12:976–89. <https://doi.org/10.1016/j.nicl.2016.05.002>.
  59. Scanlon C, Mueller SG, Cheong I, Hartig M, Weiner MW, Laxer KD. Grey and white matter abnormalities in temporal lobe epilepsy with and without mesial temporal sclerosis. *J Neurol.* 2013;260:2320–9. <https://doi.org/10.1007/s00415-013-6974-3>.
  60. Riederer F, Lanzenberger R, Kaya M, Prayer D, Serles W, Baumgartner C. Network atrophy in temporal lobe epilepsy: a voxel-based morphometry study. *Neurology.* 2008;71:419–25. <https://doi.org/10.1212/01.wnl.0000324264.96100.e0>.
  61. Kikuchi K, Togao O, Yamashita K, Momosaka D, Nakayama T, Kitamura Y, et al. Diagnostic accuracy for the epileptogenic zone detection in focal epilepsy could be higher in FDG-PET/MRI than in FDG-PET/CT. *Eur Radiol.* 2021;31:2915–22. <https://doi.org/10.1007/s00330-020-07389-1>.
  62. Guo K, Cui B, Shang K, Hou Y, Fan X, Yang H, et al. Assessment of localization accuracy and postsurgical prediction of simultaneous (18)F-FDG PET/MRI in refractory epilepsy patients. *Eur Radiol.* 2021. <https://doi.org/10.1007/s00330-021-07738-8>.
  63. Guo K, Wang J, Wang Z, Wang Y, Cui B, Zhao G, et al. Morphometric analysis program and quantitative positron emission tomography in presurgical localization in MRI-negative epilepsies: a simultaneous PET/MRI study. *Eur J Nucl Med Mol Imaging.* 2022;49:1930–8. <https://doi.org/10.1007/s00259-021-05657-w>.
  64. Li Y, Zhang T, Feng J, Qian S, Wu S, Zhou R, et al. Processing speed dysfunction is associated with functional corticostriatal circuit alterations in childhood epilepsy with centrotemporal spikes: a PET and fMRI study. *Eur J Nucl Med Mol Imaging.* 2022;49:3186–96. <https://doi.org/10.1007/s00259-022-05740-w>.
  65. Yuan S, Huang H, Cai B, Li J, Zhang M, Luo J. Altered metabolic-functional coupling in the epileptogenic network could predict surgical outcomes of mesial temporal lobe epilepsy. *Front Neurosci.* 2023;17:1165982. <https://doi.org/10.3389/fnins.2023.1165982>.
  66. Zhang M, Huang H, Liu W, Tang L, Li Q, Wang J, et al. Combined quantitative T2 mapping and [(18)F]FDG PET could improve lateralization of mesial temporal lobe epilepsy. *Eur Radiol.* 2022;32:6108–17. <https://doi.org/10.1007/s00330-022-08707-5>.
  67. Shang K, Wang J, Fan X, Cui B, Ma J, Yang H, et al. Clinical value of hybrid TOF-PET/MR imaging-based multiparametric imaging in localizing seizure focus in patients with MRI-Negative temporal lobe epilepsy. *AJNR Am J Neuroradiol.* 2018;39:1791–8. <https://doi.org/10.3174/ajnr.A5814>.
  68. Moffett JR, Ross B, Arun P, Madhavarao CN, Namboodiri AM. N-Acetylaspartate in the CNS: from neurodiagnostics to neurobiology. *Prog Neurobiol.* 2007;81:89–131. <https://doi.org/10.1016/j.pneurobio.2006.12.003>.
  69. Moffett JR, Arun P, Ariyannur PS, Namboodiri AM. N-Acetylaspartate reductions in brain injury: impact on post-injury neuroenergetics, lipid synthesis, and protein acetylation. *Front Neuroenergetics.* 2013;5:11. <https://doi.org/10.3389/fnene.2013.00011>.
  70. Clark JF, Doepke A, Filosa JA, Wardle RL, Lu A, Meecker TJ, et al. N-acetylaspartate as a reservoir for glutamate. *Med Hypotheses.* 2006;67:506–12. <https://doi.org/10.1016/j.mehy.2006.02.047>.
  71. Zhang L, Guo Y, Hu H, Wang J, Liu Z, Gao F. FDG-PET and NeuN-GFAP immunohistochemistry of hippocampus at different phases of the pilocarpine model of temporal lobe epilepsy. *Int J Med Sci.* 2015;12:288–94. <https://doi.org/10.7150/ijms.10527>.

**Publisher's Note** Springer Nature remains neutral with regard to jurisdictional claims in published maps and institutional affiliations.

Springer Nature or its licensor (e.g. a society or other partner) holds exclusive rights to this article under a publishing agreement with the author(s) or other rightsholder(s); author self-archiving of the accepted manuscript version of this article is solely governed by the terms of such publishing agreement and applicable law.